ESI

Monodentate hydroxide as a super strong yet reversible active site for CO_2 capture from high-humidity flue gas

Pei-Qin Liao, Huayao Chen, Dong-Dong Zhou, Si-Yang Liu, Chun-Ting He, Zebao Rui, Hongbing Ji, Jie-Peng Zhang* and Xiao-Ming Chen

MOE Key Laboratory of Bioinorganic and Synthetic Chemistry, School of Chemistry and Chemical Engineering, Sun Yat-Sen University, Guangzhou 510275, China.

*E-mail: zhangjp7@mail.sysu.edu.cn

Supplementary Index

Experimental details.

Materials and General Methods. Reagents and solvents were commercially available and were used without further purification. The ligand H_2bbta was synthesized according to the literature method.[H. Hart, D. Ok, *J. Org. Chem.* **1986**, *51*, 979.] The concentration of hydrochloric acid is 12 M, and the concentration of H_2O_2 is 8.8 M. Thermogravimetric analyses were performed under N_2 with temperature increased with 10 ^oC min^{-1} using a TA-Q50 system. PXRD patterns were collected (0.02 ^{o}/step, 0.06 seconds/step) on a Bruker D8 Advance diffractometer (Cu Kα) at room temperature. XPS measurements were performed with a VG Scientific ESCALAB 250 instrument. Magnetic susceptibility measurements were performed with a Quantum Design MPMS-XL7 SQUID instrument. Electron paramagnetic resonance (EPR) measurements were performed at 9.7 GHz (X-band) using a Bruker BioSpin A300 spectrometer at 77 K. The spin concentrations in the samples were determined from the second integral of the spectra using $CuSO_4{\cdot}5H_2O$ as a standard. Differential scanning calorimetry (DSC) measurements were performed in the temperature range 313-383 K on a TA-Q2000 DSC instrument. Diffused Reflection Fourier Transform Infrared Spectra (DR-FTIR) were measured by a Bruker VERTEX 70 spectrometer in the 400–4000 cm^{-1} region.

Synthesis of $[Mn_2Cl_2(bbta)]$ (1 or MAF-X25). A mixture of $MnCl_2{\cdot}4H_2O$ (0.050 g, 0.252 mmol) and H_2bbta (0.020 g, 0.126 mmol) was dissolved in a 100:100:1 (*v*/*v*/*v*) mixture of DMF-methanol-HCl (8 mL) in a 15-mL Teflon reactor, which was heated in an oven at 70 °C for 72 h and then cooled to room temperature at a rate of 5 °C h^{-1}. The obtained mixture was filtered, successively washed by H_2O and MeOH twice, soaked in MeOH for two days, filtered, and finally heated at 100 ^oC for 10 h to give light purple microcrystalline powder (yield 72% based on H_2bbta). See Table S3 for elementary analysis.

Synthesis of $[Mn_2Cl_2(bbta)(OH)]$ (1' or MAF-X25ox). A solution of H_2O_2 (0.5 mmol) in water (10 mL) was slowly added in 12 h to a suspension of **1** (0.0169 g, 0.05 mmol) in a mixed solvent of CH_3CN (5.0 mL), water (5.0 mL), and triethylamine (0.02 mL) at 0 °C under stirring, during which the color of the suspension turned brown gradually. The mixture was further stirred for 2 days at room temperature, and then filtered, washed by CH_3CN and dried in N_2 flow, and finally heated at 100 ^oC for 10 h to give dark green microcrystalline powder (0.0152 g, yield 97%). See Table S3 for elementary analysis.

Synthesis of $[Co_2Cl_2(bbta)]$ (2 or MAF-X27). A mixture of $CoCl_2{\cdot}6H_2O$ (0.030 g, 0.126 mmol), H_2bbta (0.020 g, 0.126 mmol) was dissolved in a 100:100:1 (*v*/*v*/*v*) mixture of DMF-methanol-HCl (8 mL) in a 15-mL Teflon reactor, which was heated in an oven at 70 °C for 72 h and then cooled to room temperature at a rate of 5 °C h^{-1}. The obtained mixture was filtered, successively washed by H_2O and MeOH twice, soaked in MeOH for two days, filtered, and finally heated at 100 ^oC for 10 h to give pink microcrystalline powder (yield: 85%). See Table S3 for elementary analysis.

Synthesis of $[Co_2Cl_2(bbta)(OH)]$ (2' or MAF-X27ox). A solution of H_2O_2 (0.5 mmol) in water (10 mL) was slowly added in 12 h to a suspension of **2** (0.0171 g, 0.05 mmol) in CH_3CN (5.0 mL), water (5.0 mL), and triethylamine (0.02 mL) at 0 °C under stirring, during which the color of the suspension turned from red to brown-red gradually. The mixture was further stirred for 12 h at room temperature, and then filtered, washed by CH_3CN and dried in N_2 flow, and finally heated at 100 ^oC for 10 h to give yellow microcrystalline powder (0.0156 g, yield 98%). See Table S3 for elementary analysis.

X-ray Crystallography. Because single-crystal specimen cannot be obtained for **2** or **2'** so far, their crystal structures were solved by the Rietveld refinement of their powder X-ray diffraction data. To confirm the good crystallinity and purity of all samples, the Rietveld refinement was also applied to microcrystalline samples of **1** and **1'**. The microcrystalline samples were placed in a glass capillary (Φ = 0.70 mm), and heated under high vacuum at 373 K for 24 h. After that, the capillary was sealed by a torch. The PXRD patterns were collected (0.02 ^{o}/step, 10 seconds/step) on a Bruker D8 Advance diffractometer (Cu Kα) at room temperature.

Pawley and Rietveld refinements were performed by the Reflex plus module of Material Studio. Pawley refinements were performed in the 2θ range of 6–70^{o} on unit-cell parameters, zero point and background terms with Pseudo-Voigt profile function and Berar-Baldinozzi asymmetry correction function under the *R*-3*m* space group, yielding the following parameters: a = 25.39(2) Å, c = 8.543(7) Å, R_p = 1.79%, R_{wp} = 2.41% for **1**, a = 24.60(1) Å, c = 8.320(4) Å, R_p = 0.70%, R_{wp} = 1.35% for **1'**, a = 24.739(19) Å, c = 8.179(6) Å, R_p = 0.73%, R_{wp} = 1.25% for **2** and a = 24.086(30) Å, c = 7.804(10) Å, R_p = 0.54%, R_{wp} = 0.80% for **2'**. Rietveld refinements were performed in the 2θ range of 6−70 degree. The initial structural models were produced by referring the reported single-crystal structure of **1**. In each refinement, the structures of **1**/**2** and **1'**/**2'** were divided into 3 (metal ion, chloride ion, and organic ligand) and 4 (metal ion, chloride ion, organic ligand, and hydroxide) rigid fragments that allowed for motion. These structural freedoms (including the occupancy of the hydroxide anion) together with the pseudo-Voigt profile parameters, background parameters, the cell parameters, the zero point of the diffraction pattern, the global isotropic atom displacement parameters, the Berar–Baldinozzi asymmetry correction parameters, and the March–Dollase preferred orientation correction parameters, were optimized step by step to improve the agreement between the calculated and the experimental powder diffraction patterns. The refinements gave hydroxide occupancies of 0.46 for **1'** and 0.47 for **2'**, which were similar to those evaluated by the N_2 isotherm, XPS, and/or magnetic susceptibility measurements (The $\chi_m T$ products of each Co(II) at 300 K of **2** and **2'** are 2.57 and 1.42 cm^3 K mol^{-1} ($\chi_m T$ product of low-spin Co(III) is zero) respectively, indicating that Co(III) ion in **2'** is about 45%. On the other hand, since both Mn(II) and Mn(III) are paramagnetic with multiple unpaired electrons, their relative ratio can be hardly determined by magnetic susceptibility.). Finally, the occupancies of hydroxide were fixed as 0.5, and other parameters were continued to be optimized until the best agreement between the calculated and the experimental powder diffraction patterns (Figure S1). Crystal data were summarized in Table S2.

Gas Sorption Measurements. The sorption isotherms were measured with automatic volumetric adsorption apparatuses (Micromertics ASAP 2020M and BELSORP-max). The as-synthesized sample (weight of about 100−200 mg) was placed in the sample tube and dried for 12 h at 100 °C to remove the remnant solvent molecules prior to measurements. Ultrahigh-purity-grade (99.999%) N_2 and CO_2 were used for all measurements. The temperatures were controlled by a liquid-nitrogen bath (77 K) or a water bath (298, 308, 313, 318 and 328 K).

CO_2/N_2 breakthrough curve measurements. A stainless-steel column with a length of 10 cm and an internal diameter of 0.46 cm (V_{column} = 0.230×0.230×3.14×10.0 = 1.66 cm^3) was packed with microcrystalline sample (Scheme S1). The column contained 1.574 g of **2'** or 1.424 g of **2**, corresponding to apparent densities of 0.948 and 0.858 g cm^{-3}, and column voidages of 1-0.948/1.354 = 0.300 and 1-0.858/1.138 = 0.246, respectively. The column was connected to the injection and sampling ports by stainless-steel pipes with a combined length of 40 cm and an internal diameter of 0.30 cm (V_{tube} = 0.150×0.150×3.14×40 = 2.84 cm^3). The column and most parts of the pipelines between the injection and sampling ports were placed in a temperature-controlling oven. The flow rates (mL min^{-1} at 298.15 K and 101.325 kPa) of pure gases were regulated by mass flow controllers. Before breakthrough experiments, the columns were activated by passing He (10 mL min^{-1}) and heated at 373 K for 10 hours, and then cooled to the measurement temperature of 313(1) K. Pure N_2 (1.8 mL min^{-1}) and CO_2 (0.2 mL min^{-1}) were mixed and then used directly as dry (0% RH) or passed through a water vapor saturator at 310 K as wet (82(3)% RH) gas mixture for the injection port. Prior to the breakthrough measurements in the presence of high humidity, wet He was introduced to the adsorbent bed until water saturation was detected. Then the wet He was switched to wet 10:90 CO_2/N_2 mixture to start the breakthrough experiment. The temperature and realative humidity was measured by a digital temperature-humidity sensor. The gas stream at the outlet of the column was analyzed on line by using a chromatographic analyzer (Agilent 7890A) with a TCD detector and a PLOT/Q column. Before injection of CO_2/N_2 mixture, the column and pipeline contained He of V = 1.66×0.30 + 1.574/1.354×54% + 2.84 = 3.97 cm^3, i.e., 3.97×0.1×273/313/22.4/1.574 = 0.00982 mmol g^{-1} for **2'**; or V = 1.66×0.246 + 0.754/1.138×54% + 2.84 = 3.61 cm^3, i.e., 3.61×0.1×273/313/22.4/1.424 = 0.00987 mmol g^{-1} for **2**.

The amount of CO_2 (q) retained by the column at a particular specific injection amount τ, can be calculated by

$$q(\tau) = 0.1*(\tau - \int_0^{\tau} f(\tau)\mathrm{d}\tau)$$

where the breakthrough curve is expressed by the function $f(\tau)$.

The CO_2 adsorbed by the adsorbent in the column (Q) can be calculated by

$$Q = q - q_c$$

where the q_c is the gas part of the column and the gas in the pipeline.

For example, integration of the experimental breakthrough curve of CO_2 for **2'**, either at 0% or 82(3)% RH, indicate that q reaches saturation of 2.49 mmol g^{-1} when τ > 28 mmol g^{-1}; so that Q = 2.49 – 0.01 = 2.48 mmol g^{-1}.

Calculation of approximate regeneration energy. The specific heat (1.4 J g^{-1} K^{-1}) of **2'** was measured by DSC. The sensible heat required for regeneration (98 J g^{-1}) is the specific heat (1.4 J g^{-1} K^{-1}) multiplied by the temperature change (70 K, see Fig. S18). The working capacity was obtained as 2.0 mmol g^{-1} between 15:85 CO_2/N_2 (v/v) mixture at 313 K and a pure CO_2 flow at 383 K. To remove this CO_2, approximately 144 J g^{-1} (obtaining via the integration of the coverage-dependent CO_2 adsorption enthalpy curve) are required. To adsorb 1 kg (22.72 mol) of CO_2, 11 kg of **2'** are necessary. Thus, the regeneration energy is:

11 kg* (98 kJ kg^{-1}+ 144 kJ kg^{-1}) = 2.7 MJ kg^{-1} CO_2.

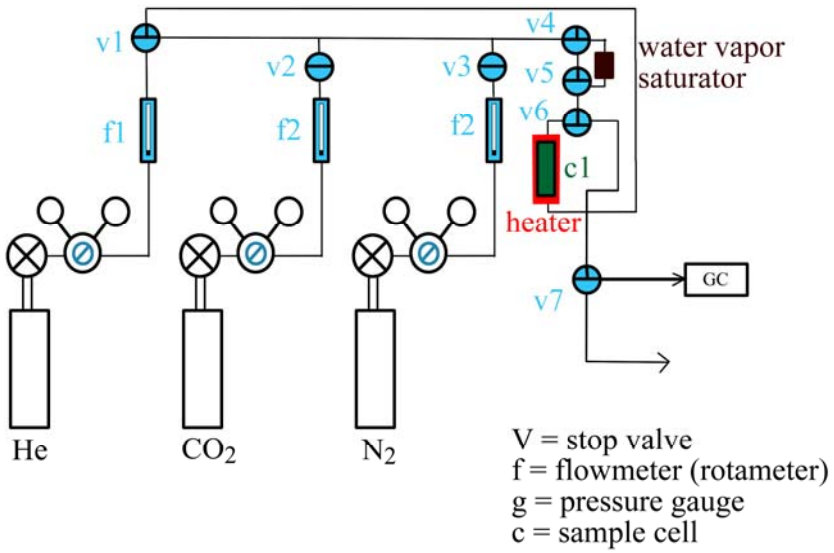

Scheme S1. Representation of the column breakthrough experiment.

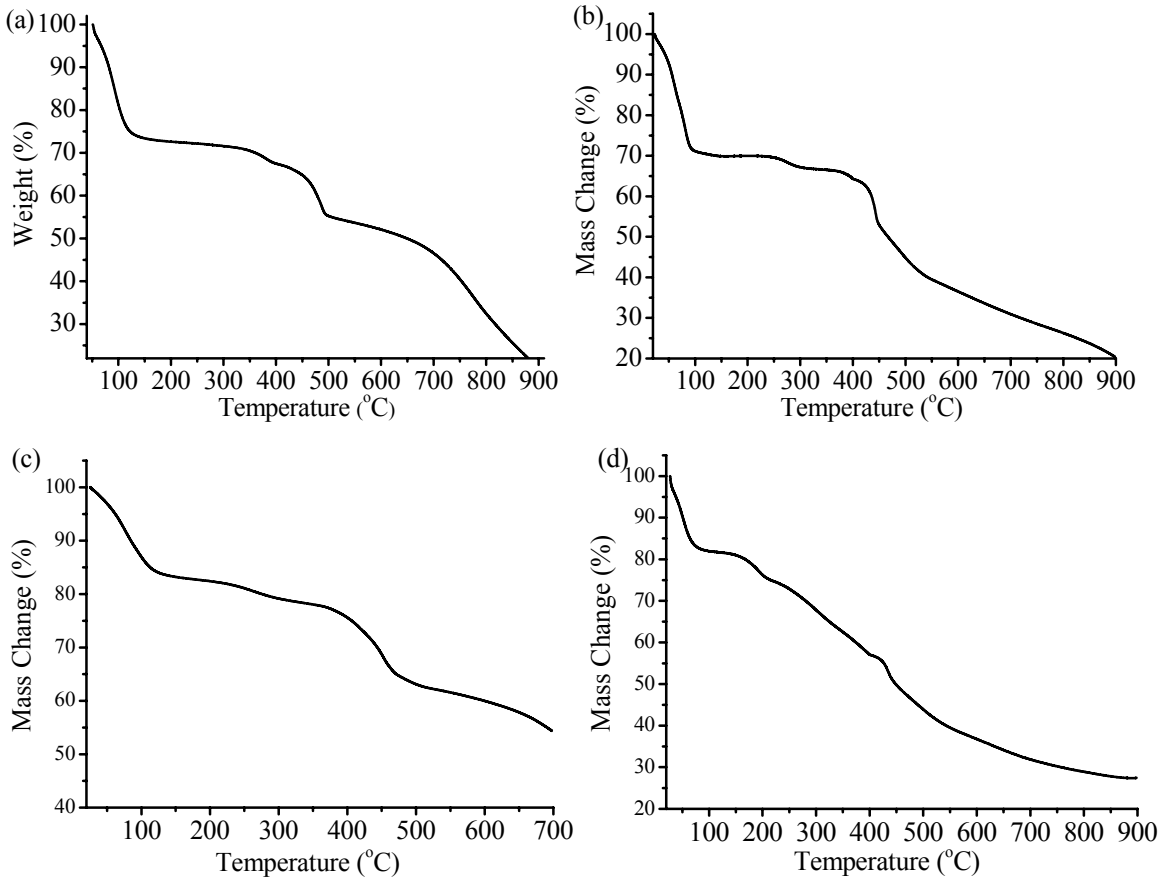

Figure S1. (a-d) TG curves of **1**, **2**, **1'** and **2'**.

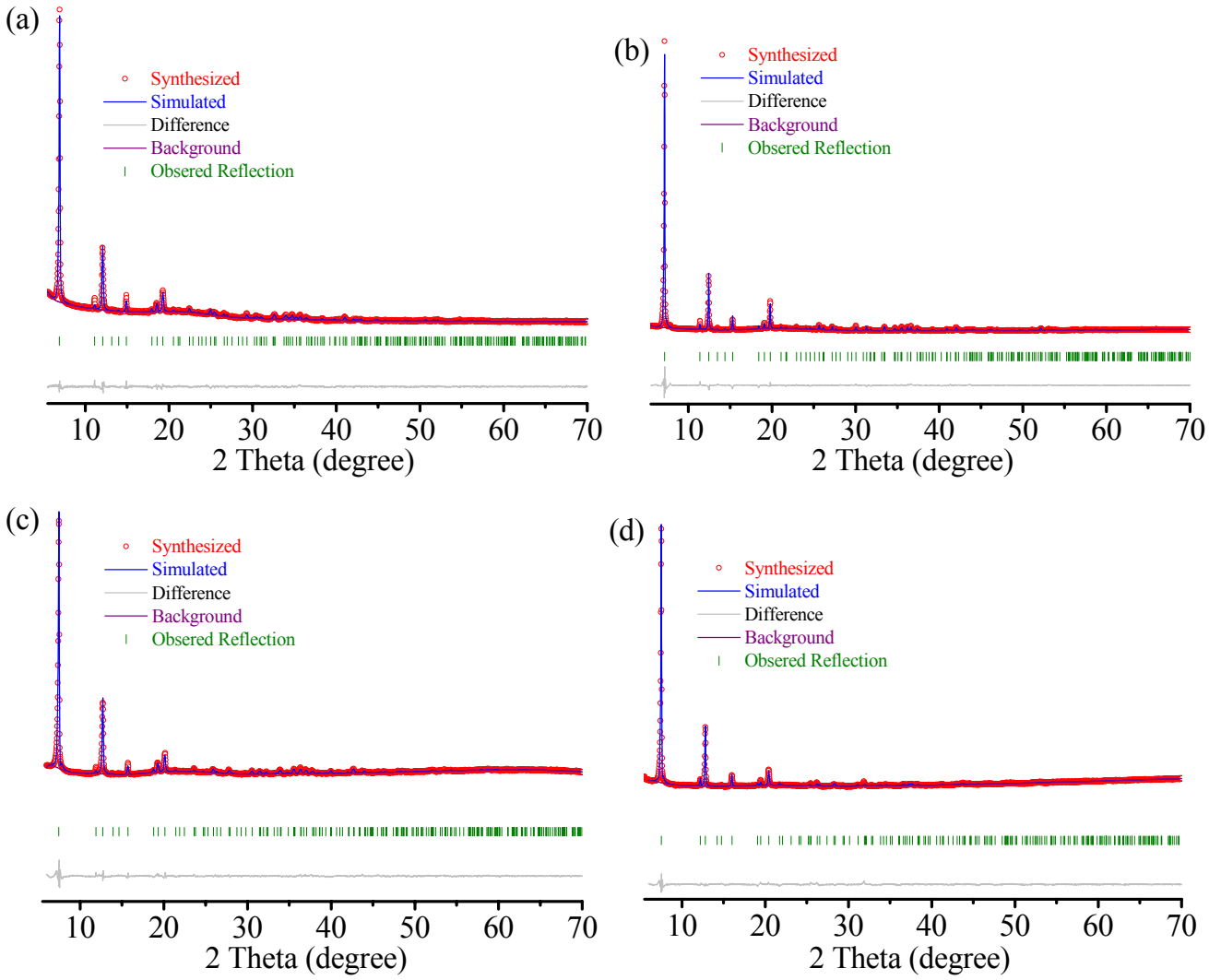

Figure S2. Rietveld refinement plot of (a) **1**, (b) **1'**, (c) **2**, and (d) **2'**. Before measurement of the PXRD data, the samples were heated at 373 K, respectively, according to the thermogravimetry curves as shown in Figure S1.

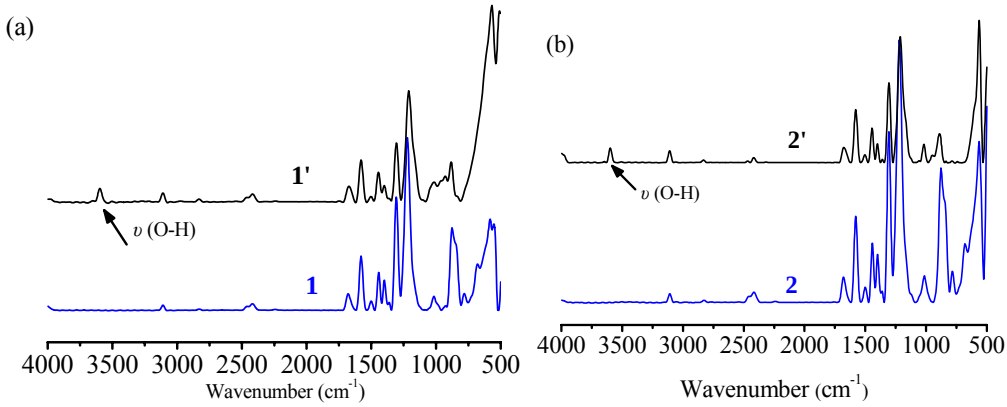

Figure S3. IR spectra of (a) **1**/**1'** and (b) **2**/**2'**. The samples were in situ desolvated before measurement.

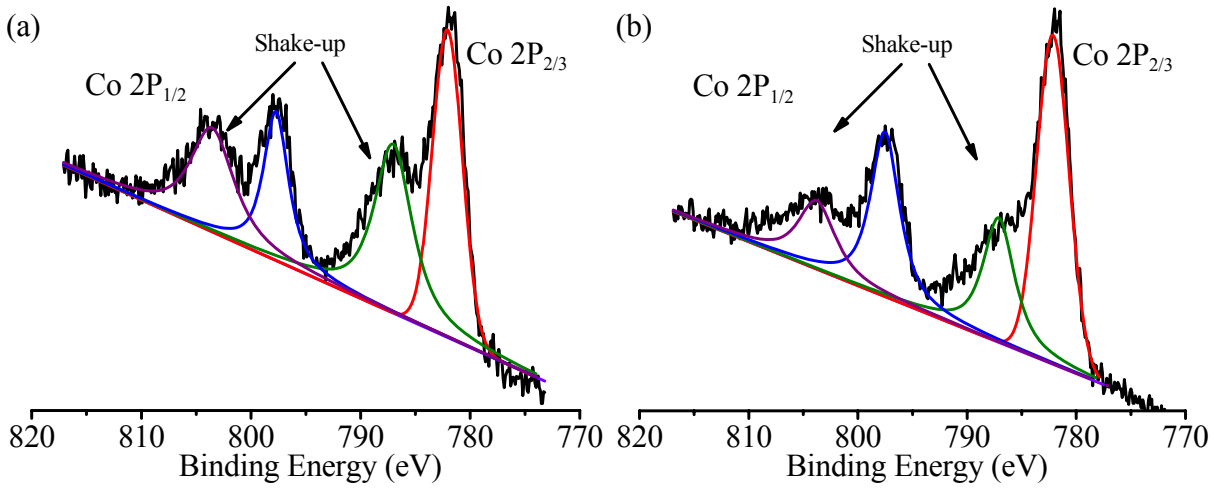

Figure S4. XPS spectra of (a) **2** and (b) **2'**. The binding energies of Co $2P_{2/3}$ (781.7 eV) and Co $2P_{1/2}$ (797.4 eV) as well as the shake-up satellite peaks in the XPS of **2** confirm the oxidation state of +2 for cobalt.[Biesinger, M. C. *et al. Appl. Surf. Sci.* **2011**, *257*, 2717] The ratio of peak areas (deconvoluted by the Gaussian-Lorentzian function) between the shake-up satellite peak (781.7 eV) and its main peak at 797.4 eV is 1.2 for **2** and 0.53 for **2'**, indicating that the proportion of Co(III) ion in **2'** is about 55%.

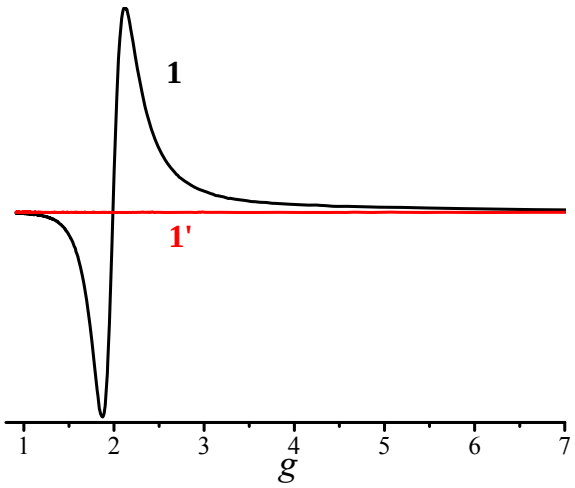

Figure S5. EPR spectra of **1** (black) and **1'** (red). The strong broad EPR signal with g = 1.997 demonstrated that the presence of Mn(II) species in **1**. On the other hand, the EPR spectrum of 1' was silent, indicating the presence of Mn(III) in **1'**. The EPR signal of Mn(II) in **1'** was not observed, which could be attributed to the relatively high measurement temperature (77 K) and the changed coordination environment.

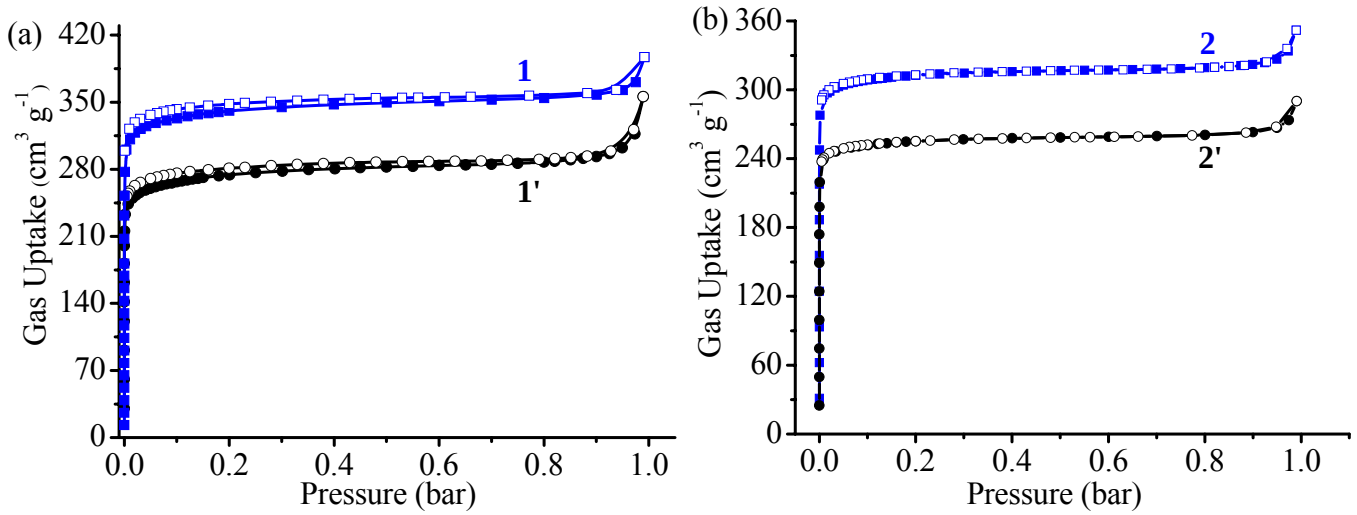

Figure S6. N_2 isotherms measured at 77 K. Assuming the oxidation ratio is 100%, the crystallography pore volumes of **1'** and **2'** can be calculated as 0.38 $cm^3\ g^{-1}$ (void = 48.4%, D_c = 1.285 g cm^{-3}) and 0.32 $cm^3\ g^{-1}$ (void = 46.8%, D_c = 1.452 g cm^{-3}), corresponding to saturated N_2 uptakes of 243 and 205 $cm^3\ g^{-1}$, respectively. Assuming the oxidation ratio of 50%, the crystallography pore volumes of **1'** and **2'** were 0.44 $cm^3\ g^{-1}$ and 0.40 $cm^3\ g^{-1}$, corresponding to saturated N_2 uptakes of 282 and 256 $cm^3\ g^{-1}$, respectively (Table S2).

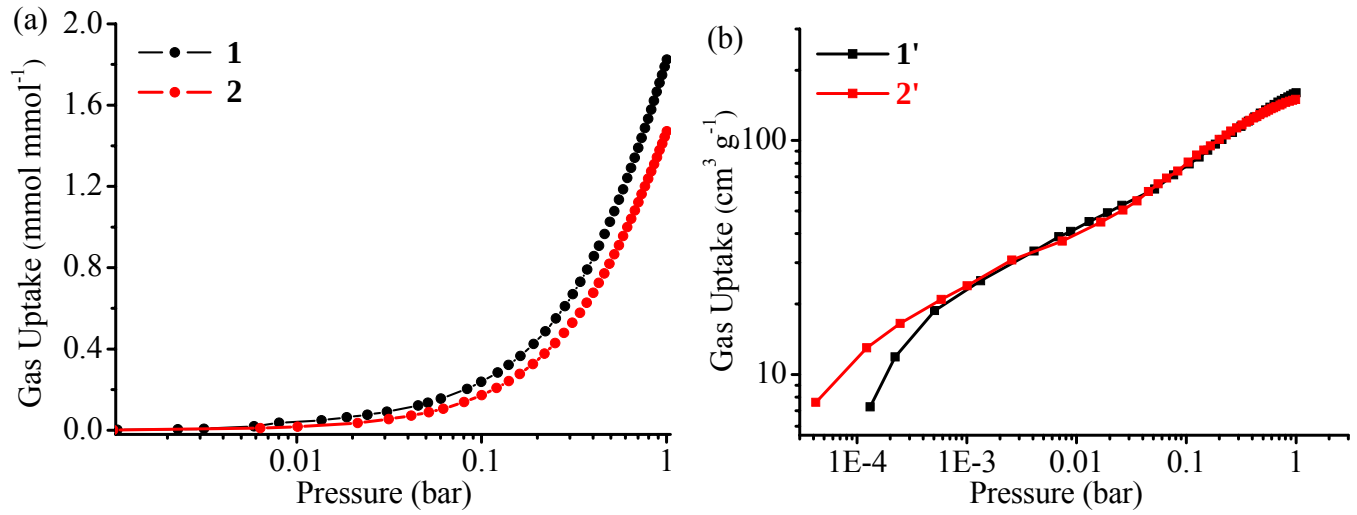

Figure S7. Comparison of the CO_2 adsorption isotherms between **1** and **2** and between **1'** and **2'** measured at 298 K.

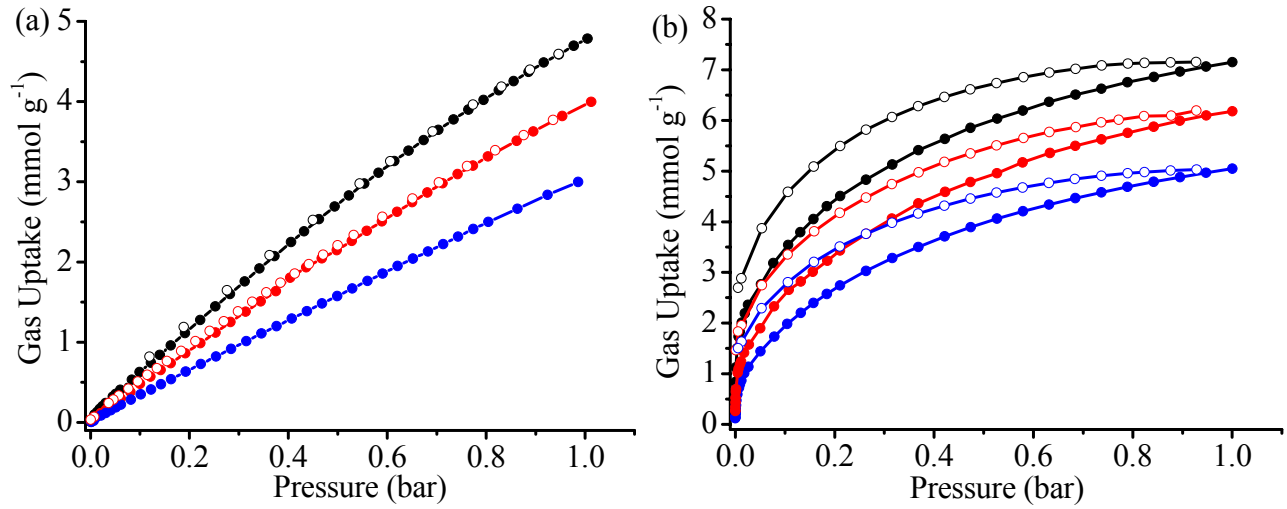

Figure S8. (a) CO_2 adsorption (solid) and desorption (open) isotherms of (a) **1** measured at 298 (black), 308 (red) and 318 K (blue) and (b) **1'** measured at 298 (black), 313 (red) and 328 K (blue).

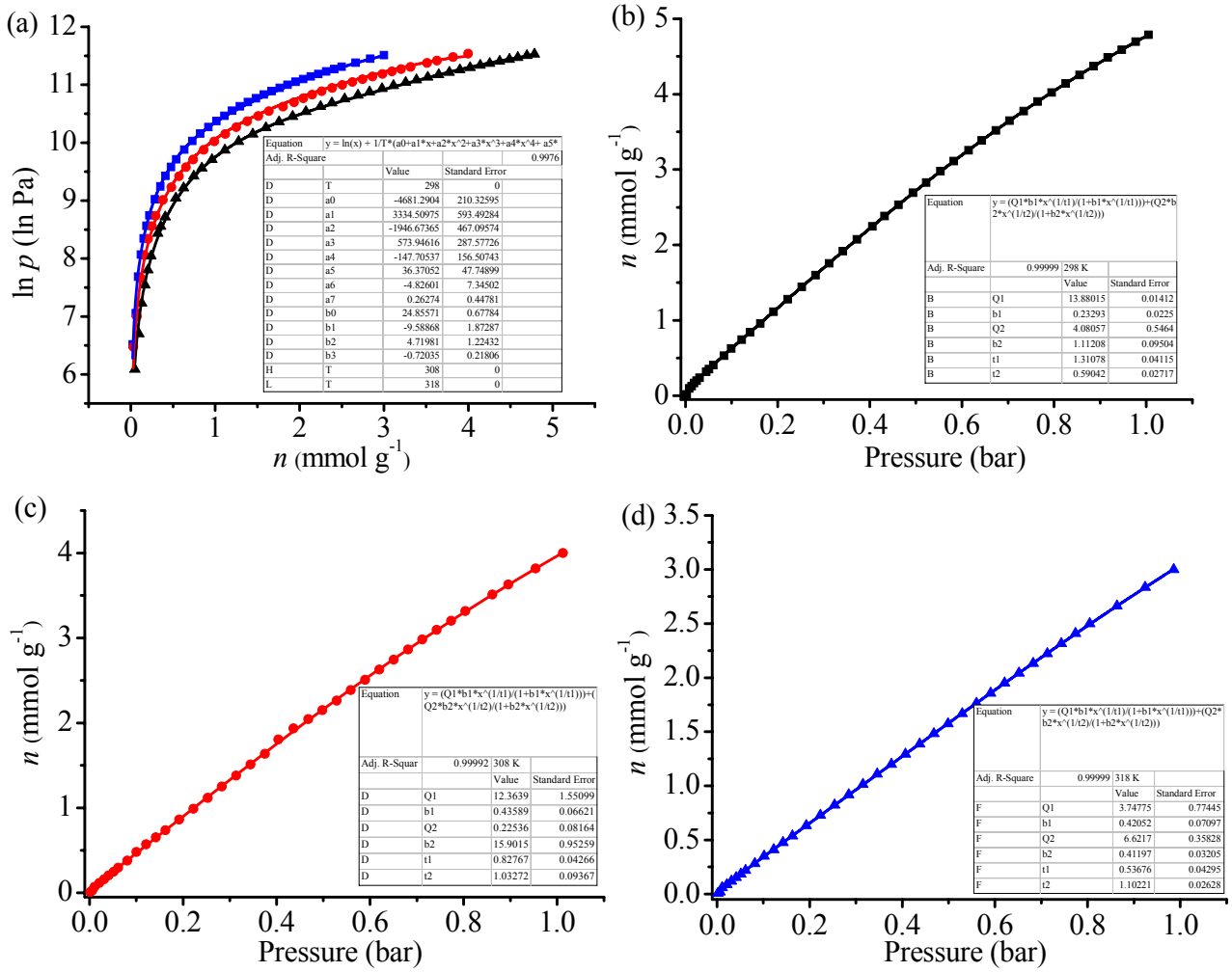

Figure S9. (a) Virial fitting (lines) of the CO_2 adsorption isotherms (points) of **1** measured at 298 (black), 308 (red) and 318 K (blue). (b-d) Dual-site Langmuir-Freundlich fitting (lines) of the CO_2 adsorption isotherms (points) of **1** measured at 298 (black), 308 (red) and 318 K (blue).

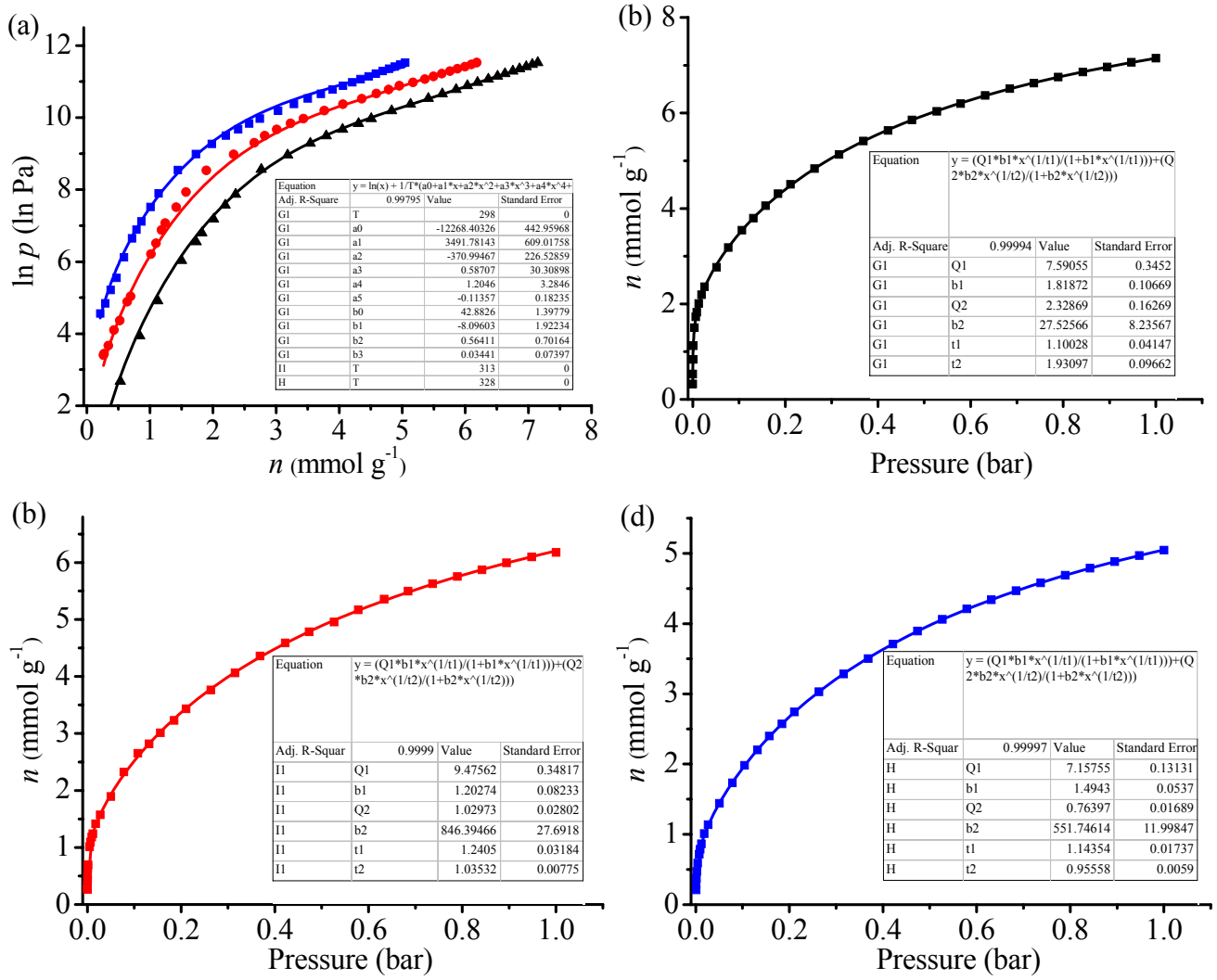

Figure S10. (a) Virial fitting (lines) of the CO_2 adsorption isotherms (points) of **1'** measured at 298 (black), 313 (red) and 328 K (blue). (b-d) Dual-site Langmuir-Freundlich fitting (lines) of the CO_2 adsorption isotherms (points) of **1'** measured at 298 (black), 313 (red) and 328 K (blue).

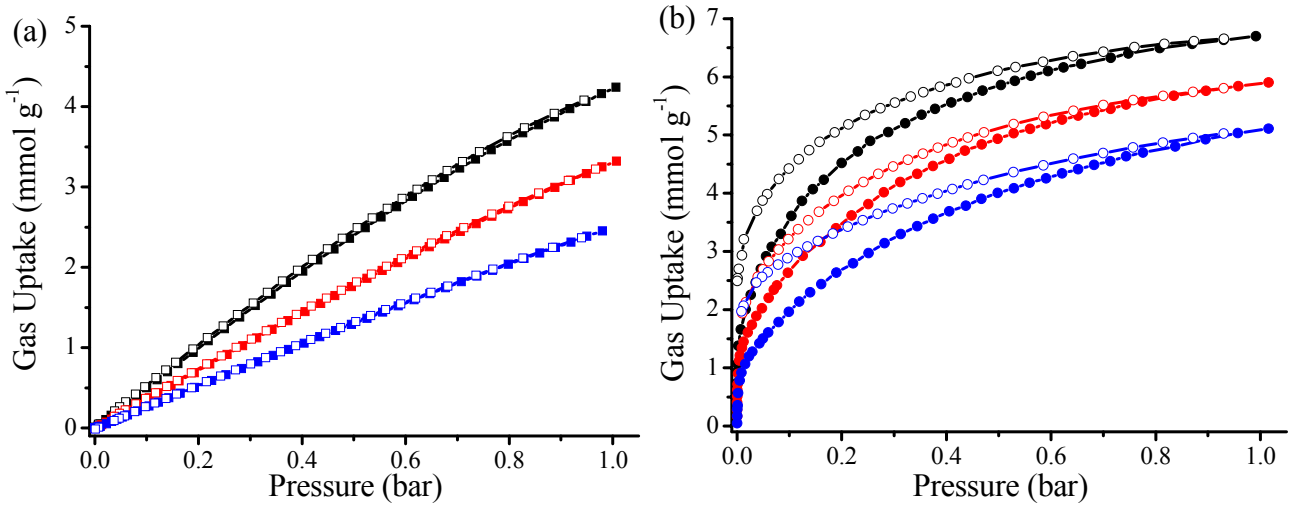

Figure S11. (a) CO_2 adsorption (solid) and desorption (open) isotherms of **2** (a) measured at 298 (black), 308 (red) and 318 K (blue) and **2'** (b) measured at 298 (black), 313 (red) and 328 K (blue).

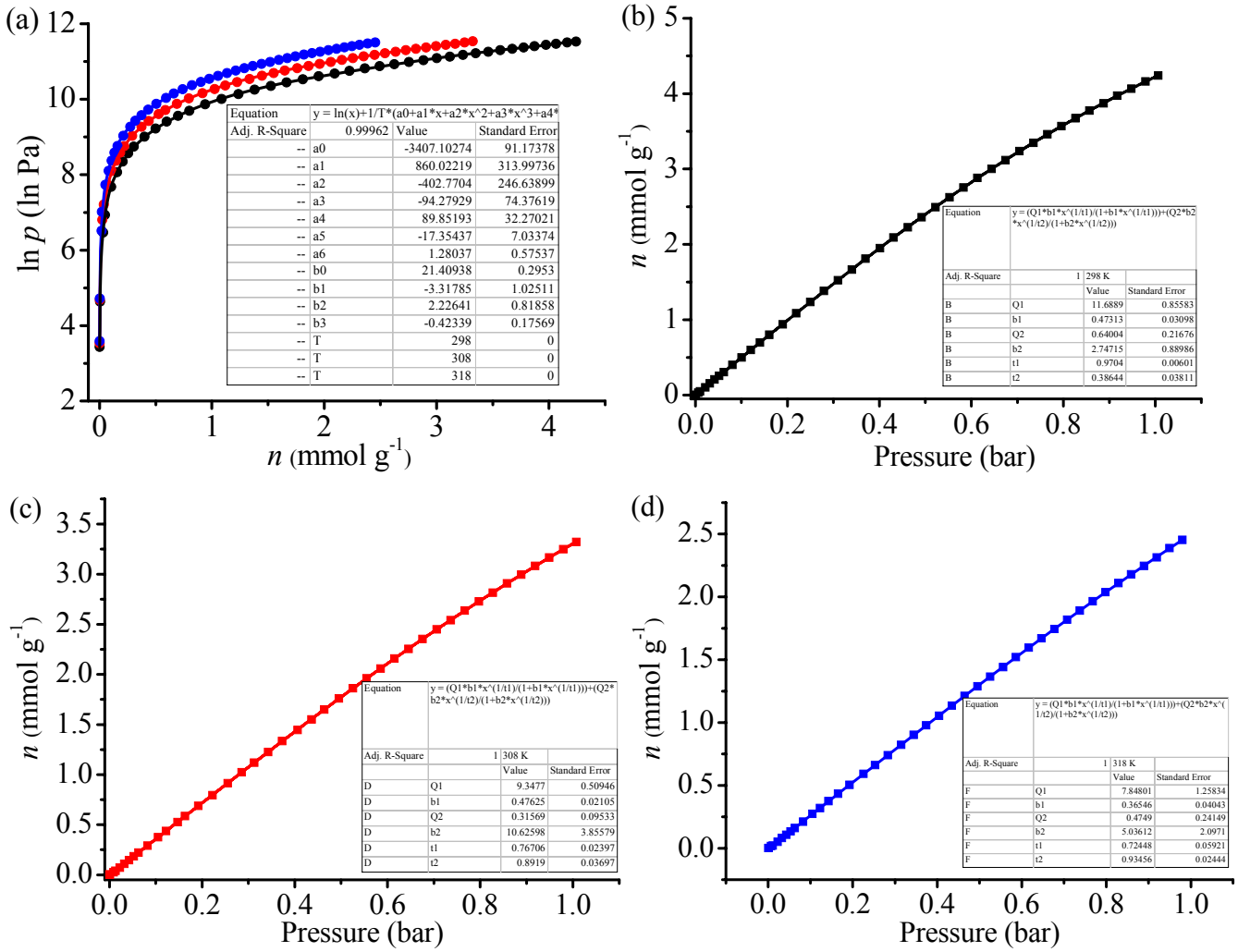

Equation	y = ln(x)+1/T*(a0+a1*x+a2*x^2+a3*x^3+a4*		
Adj. R-Square	0.99962	Value	Standard Error
--	a0	-3407.10274	91.17378
--	a1	860.02219	313.99736
--	a2	-402.7704	246.63899
--	a3	-94.27929	74.37619
--	a4	89.85193	32.27021
--	a5	-17.35437	7.03374
--	a6	1.28037	0.57537
--	b0	21.40938	0.2953
--	b1	-3.31785	1.02511
--	b2	2.22641	0.81858
--	b3	-0.42339	0.17569
--	T	298	0
--	T	308	0
--	T	318	0

Equation	y = (Q1*b1*x^(1/t1)/(1+b1*x^(1/t1)))+(Q2*b2*x^(1/t2)/(1+b2*x^(1/t2)))		
Adj. R-Square	1	298 K	
		Value	Standard Error
B	Q1	11.6889	0.85583
B	b1	0.47313	0.03098
B	Q2	0.64004	0.21676
B	b2	2.74715	0.88986
B	t1	0.9704	0.00601
B	t2	0.38644	0.03811

Equation	y = (Q1*b1*x^(1/t1)/(1+b1*x^(1/t1)))+(Q2*b2*x^(1/t2)/(1+b2*x^(1/t2)))		
Adj. R-Square	1	308 K	
		Value	Standard Error
D	Q1	9.3477	0.50946
D	b1	0.47625	0.02105
D	Q2	0.31569	0.09533
D	b2	10.62598	3.85579
D	t1	0.76706	0.02397
D	t2	0.8919	0.03697

Equation	y = (Q1*b1*x^(1/t1)/(1+b1*x^(1/t1)))+(Q2*b2*x^(1/t2)/(1+b2*x^(1/t2)))		
Adj. R-Square	1	318 K	
		Value	Standard Error
F	Q1	7.84801	1.25834
F	b1	0.36546	0.04043
F	Q2	0.4749	0.24149
F	b2	5.03612	2.0971
F	t1	0.72448	0.05921
F	t2	0.93456	0.02444

Figure S12. (a) Virial fitting (lines) of the CO_2 adsorption isotherms (points) of **2** measured at 298 (black), 308 (red) and 318 K (blue). (b-d) Dual-site Langmuir-Freundlich fitting (lines) of the CO_2 adsorption isotherms (points) of **2** measured at 298 (black), 308 (red) and 318 K (blue).

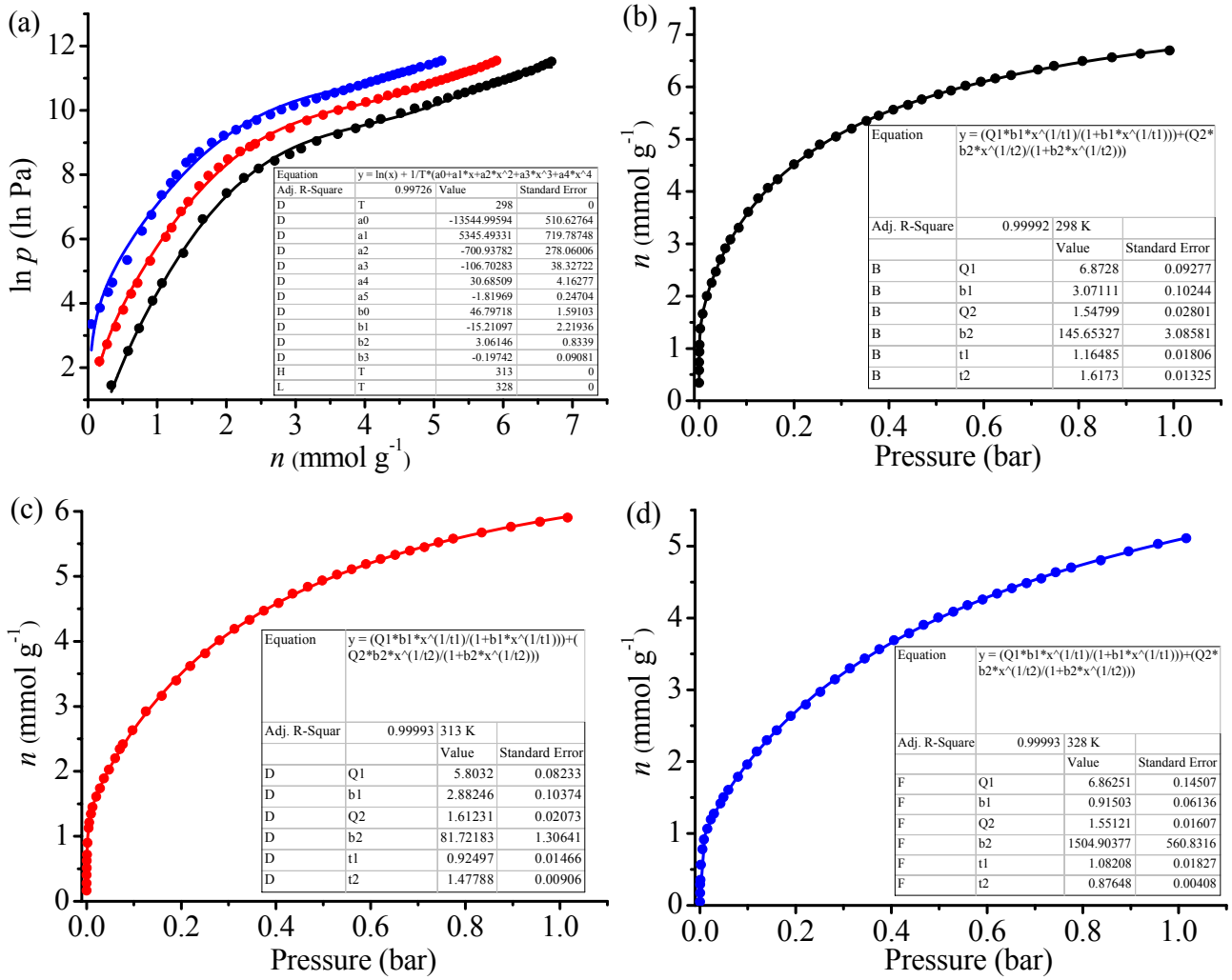

Figure S13. (a) Virial fitting (lines) of the CO_2 adsorption isotherms (points) of **2'** measured at 298 (black), 313 (red) and 328 K (blue). (b-d) Dual-site Langmuir-Freundlich fitting (lines) of the CO_2 adsorption isotherms (points) of **2'** measured at 298 (black), 313 (red) and 328 K (blue).

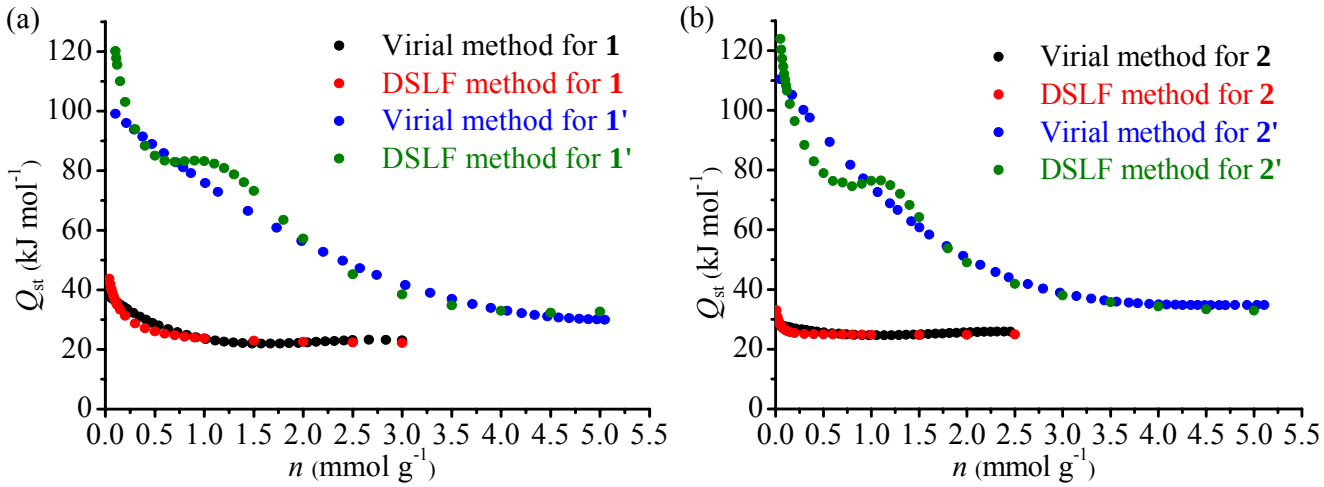

Figure S14. Comparison of the coverage-dependent CO_2 adsorption enthalpy obtained by the Virial and DSLF methods.

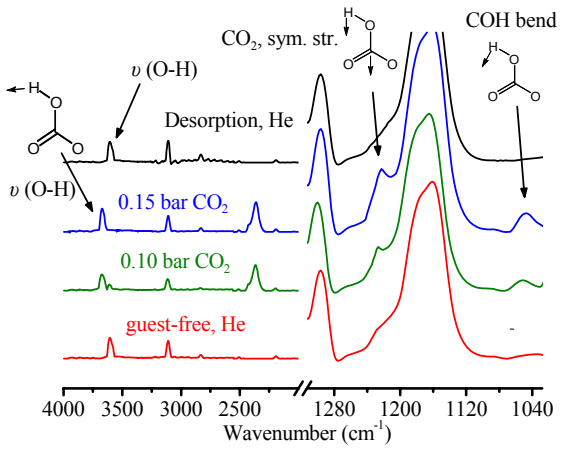

Figure S15. *In situ* IR spectra of **2'** with varied atmosphere measured at 313 K.

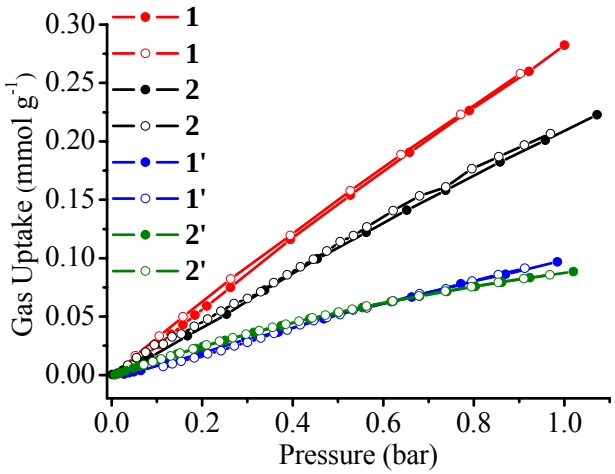

Figure S16. N_2 sorption isotherms of **1**, **2**, **1'**, and **2'** measured at 298 K.

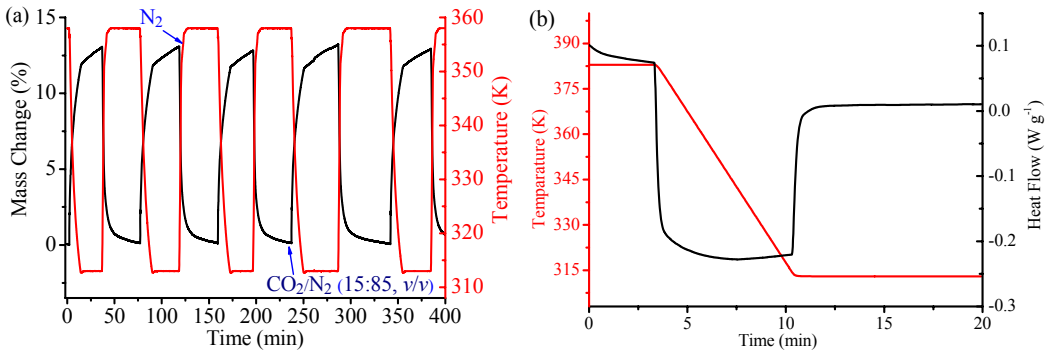

Figure S17. Repeated adsorption–desorption kinetics for **1'** between a 15:85 CO_2/N_2 (*v*/*v*) flow at 313 K and a pure N_2 flow at 358 K. (b) Heat flows from **2'**, as determined via DSC.

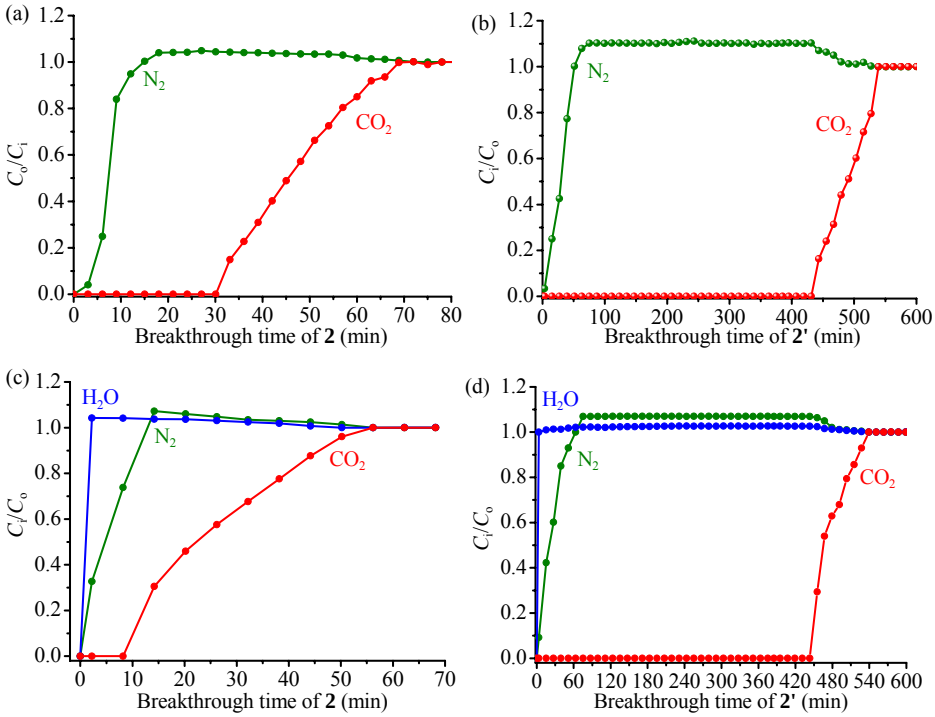

Figure S19. Breakthrough curves of Fig. 4 expressed using time (min) as abscissa.

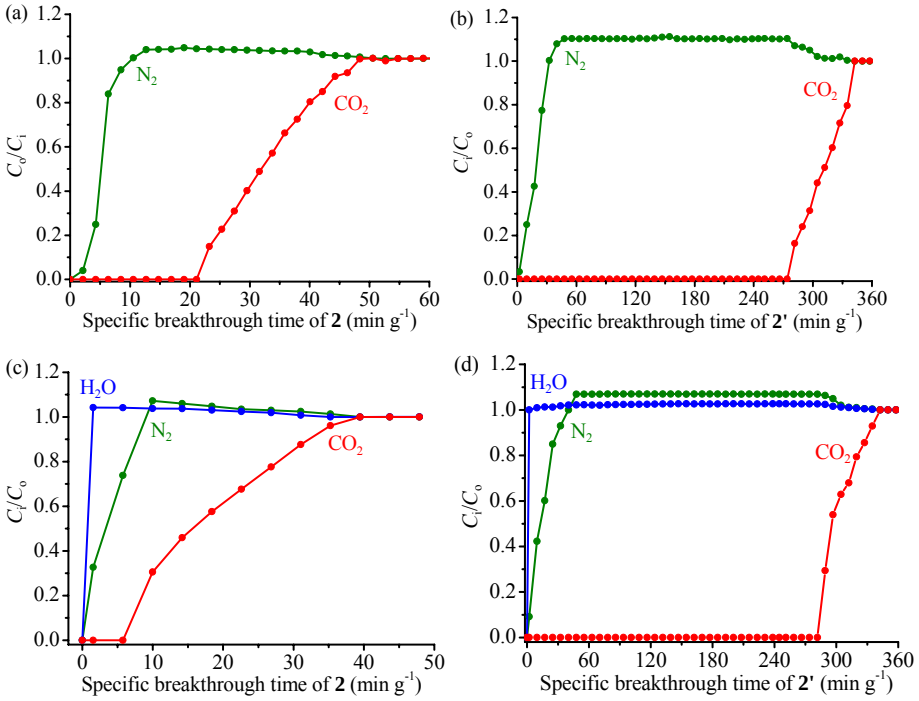

Figure S20. Breakthrough curves of Fig. 4 expressed using specific breakthrough time (min g^{-1}) as abscissa.

Table S1. Comparison of the best CO_2 adsorption performances of PCPs. Note: the highest values of each parameter were highlighted in boldface.

Compound (common name)	Q_{st} (kJ/mol)	D_c (g cm^{-3})	CO_2 uptake at 298 K and 1 atm		Selectivity[a] (298 K)	Type of active sites[i]	Ref
			mmol g^{-1}	mmol cm^{-3}			
$[Mn_2Cl_2(bbta)]$	38[g]/43[b]	1.074	5.36	5.76	26	OMS	This work
$[Co_2Cl_2(bbta)]$	28[g]/33[b]	1.138	4.24	4.82	24	OMS	This work
$[Mn_2Cl_2(bbta)(OH)]$	**99**[g]/**120**[b]	1.227	7.14	**8.76**	250	OMS+LBS	This work
$[Co_2Cl_2(bbta)(OH)]$	**110**[g]/**124**[b]	1.354	6.70	**9.07**	262	OMS+LBS	This work
CD-MOF-2	113.5[h]	0.996	2.59	2.58	NA	LBS	S1
en-Mg_2(dobpdc)	51[b]	0.955	4.57	4.36	230	OMS+LBS	S2
mmen-Mg_2(dobpdc)	71[b]	1.073	3.86	4.14	200	OMS+LBS	S3
mmen-CuBTTri	66[g]/96[f]	1.059	4.2	4.45	165	OMS+LBS	S4
SIFSIX-2-Cu-i	31.9	1.246	5.41	6.74	183	LBS	S5
CAU-1	48[c]	0.892	3.8	3.39	45[#4]	LBS	S6
Mg_2(dobdc)	47[d]	0.920	**8.04**[#1]	7.40[#1]	44[#3]	OMS	S7
MAF-35	47[b, e]	**1.357**	4.46	6.05	37	OMS	S8
bio-MOF-11	45[c]	1.234	5.0	6.17	65	LBS	S9
rht-MOF-7	45[f]	0.783	4.76	3.73	NA	OMS+LBS	S10
Mg_2(dobpdc)	44[b]	0.713	6.42	4.58	NA	OMS	S3
Cu-TDPAT	42[g]	0.782	7.94	6.21	36	OMS+LBS	S11
Ni_2(dobdc)	41[c]	1.194	5.8[#1]	6.93[#1]	30	OMS	S7
Zn_2(ox)(atz)	41[e]	1.713	3.79[#2]	6.50[#2]	NA	LBS	S12
Co_2(dobdc)	37[d]	1.177	6.96[#1]	8.20[#1]	NA	OMS	S7
HKUST-1	35[e]	0.879	4.86	4.27	101[#2]	OMS	S13
[Cu(Me-4py-trz-ia)]	30[d]	0.928	6.1[#1]	5.7	NA	OMS+LBS	S14
PCN-88	27[g]	0.657	5.5	3.64[#1]	60	OMS	S15
MAF-66	26[g]	1.128	5.0	5.6	185	LBS	S16
Cu-TPBTM	26[g]	0.627	4.72	2.96	20	OMS+LBS	S17
PEI (40 wt%)⊂ PAF-5	68.7[b]	NA	3.6	NA	**1200**	LBS	S18
PEI-MIL-101-100	NA	NA	5.00	NA	770	LBS	S19

mmen = N,N'-dimethylethylenediamine; BTTri = 1,3,5-tris(1H-1,2,3,-triazol-5-yl)benzene; dobpdc = 4,4'-dioxido-3,3'-biphenyldicarboxylate; dobdc = 2,5-dioxido-1,4-benzenedicarboxylate; TDPAT = 2,4,6-tris(3,5-dicarboxylphenyl-amino)-1,3,5-triazine; ox = oxalate; atz = 3-amino- 1,2,4-triazole; Me-4py-trz-ia = 5-(3-methyl-5-(pyridine-4-yl)-(4H-1,2,4-triazol-4-yl)isophthalate); TPBTM = N,N',N''-tris(isophthalyl)-1,3,5-benzenetricarboxamide. SIFSIX = SiF_6^{2-} anions; PEI = polyethyleneimine.

[a] The CO_2/N_2 selectivity can be calculated by several methods. To compared the practical performances of different materials, the CO_2/N_2 selectivity discussed in this work is calculated under the flue gas condition, which is equal to uptake ratio at the partial pressures of each gas devided by the pressure ratio.

[b] Obtained by the Clausius−Clapeyron equation and dual-site Langmuir−Freundlich fitting.

[c] Obtained by the Clausius−Clapeyron equation and single-site Langmuir−Freundlich fitting.

[d] Obtained by the Clausius−Clapeyron equation and Toth fitting.

[e] Obtained by the Clausius−Clapeyron equation without mathematical fitting.

[f] Obtained by the Clausius−Clapeyron equation and dual-site Langmuir fitting.

[g] Obtained by the Virial fitting method.

[h] Obtained by calorimetric methodology.

[#1] 296 K; [#2] 293 K; [#3] 303 K; [#4]273 K.

[i] LBS = Lewis basic site.

Table S2. Summary of the Crystal Data and Structure Refinement results.

Compound	**1**	**1'**	**2**	**2'**
Formula	$C_6H_2Cl_2Mn_2N_6$	$C_6H_3Cl_2Mn_2N_6O$	$C_6H_2Cl_2Co_2N_6$	$C_6H_3Cl_2Co_2N_6O$
Formula weight	338.92	355.91	346.89	363.90
Temperature (K)	293(2)	293(2)	293(2)	293(2)
Space group	*R*-3*m*	*R*-3*m*	*R*-3*m*	*R*-3*m*
a (Å)	25.40(3)	24.58(1)	24.44(3)	24.28(4)
c (Å)	8.542(8)	8.318(4)	8.088(10)	7.867(14)
V (Å^3)	4773(14)	4352(5)	4182(13)	4016(17)
Z	18	18	18	18
D_c (g cm^{-3})	1.061	1.226	1.138	1.354
μ (mm^{-1})	1.430	1.588	2.058	2.151
R_p (%)	1.96	0.98	0.75	0.58
R_{wp} (%)	2.66	1.72	1.14	0.81
M1-N1 (Å)	2.232(3)	2.088(2)	2.123(2)	2.086(2)
M1-N2 (Å)	2.167(2)	2.104(2)	2.068(2)	2.011(2)
M1-Cl1 (Å)	2.420(2)	2.371(3)	2.317(5)	2.294(2)
M1-O1 (Å)	NA	1.999(2) (Mn^{III}-OH)	NA	1.972(6) (Co^{III}-OH)
void (%)[a]	59.8	54.0	57.4	53.6
pore volume (cm^3 g^{-1}) [b]	0.56	0.44	0.50	0.40

$R_p = \Sigma|cY^{sim}(2\theta_i) - I^{exp}(2\theta_i) + Y^{back}(2\theta_i)|/\Sigma|I^{exp}(2\theta_i)|$.

$R_{wp} = \{w_p[cY^{sim}(2\theta_i) - I^{exp}(2\theta_i) + Y^{back}(2\theta_i)]^2/\Sigma w_p[I^{exp}(2\theta_i)]^2\}^{1/2}$, and $w_p = 1/I^{exp}(2\theta_i)$.

$R_1 = \sum||F_o| - |F_c||/\sum|F_o|$. $wR_2 = [\sum w(F_o^2 - F_c^2)^2/\sum w(F_o^2)^2]^{1/2}$.

[a] Calculated by the SOLV routine in Platon (Version: 131110).[A. Spek, *J. Appl. Crystallogr.* **2003**, *36*, 7]

[b] Pore volume = void / D_c.

Table S3 Elemental analyses.

Sample	C/N ratio		Carbon, %		Nitrogen, %		Hydrogen, %	
	Exp.	Calc.	Exp.	Calc.	Exp.	Calc.	Exp.	Calc.
$[Mn_2(H_2O)_2Cl_2(bbta)]\cdot 6.5H_2O$ ($C_6H_{19}Cl_2Mn_2N_6O_{8.5}$) (**1**)	0.887	0.857	14.97	14.65	16.87	17.08	3.91	3.89
$[Mn_2(OH)(H_2O)Cl_2(bbta)]\cdot 6.5H_2O$ ($C_6H_{18}Cl_2Mn_2N_6O_{8.5}$) (**1'**)	0.887	0.857	15.00	14.68	16.91	17.11	3.88	3.69
$[Co_2(H_2O)_2Cl_2(bbta)]\cdot 6H_2O$ ($C_6H_{18}Cl_2Co_2N_6O_8$) (**2**)	0.863	0.857	14.97	14.68	17.35	17.12	3.67	3.70
$[Co_2(OH)(H_2O)Cl_2(bbta)]\cdot 5.5H_2O$ ($C_6H_{16}Cl_2Co_2N_6O_{7.5}$) (**2'**)	0.864	0.857	15.17	14.98	17.56	17.47	3.351	3.353
$[Mn_2(HCO_3)(H_2O)Cl_2(bbta)]\cdot 1.7H_2O$ ($C_7H_{9.2}Cl_2Mn_2N_6O_{6.1}$) (**1'**·$CO_2$)	1.000	1.000	18.74	18.45	18.73	18.45	2.356	2.035
$[Mn_2(OH)(H_2O)Cl_2(bbta)]\cdot 6.5H_2O$* ($C_6H_{18}Cl_2Mn_2N_6O_{8.5}$) (**1'**)	0.887	0.857	15.05	14.68	16.97	17.11	3.869	3.69
$[Co_2(HCO_3)(H_2O)Cl_2(bbta)]\cdot 1.8H_2O$ ($C_7H_{8.6}Cl_2Co_2N_6O_{5.8}$) (**2'**·$CO_2$)	1.000	1.000	18.34	18.56	18.33	18.55	2.052	1.891
$[Co_2(OH)(H_2O)Cl_2(bbta)]\cdot 5.5H_2O$* ($C_6H_{16}Cl_2Co_2N_6O_{7.5}$) (**2'**)	0.865	0.857	15.18	14.98	17.55	17.47	3.351	3.353

*The sample was obtained by heating the corresponding CO_2-captured sample under high vacuum at 85 ^oC for 2 h.

Table S4. Comparing the performances of capturing CO_2 from simulated flue gas (T = 313 K, P_{CO2} = 0.15 bar) of **1'** and **2'** with the highest reported values.

Compound	Density (g cm^{-3})	Gravimetric capacity (wt %)	Volumetric capacity (mmol cm^{-3})	Regeneration condition	Q_{st} (kJ/mol)	Ref
mmen-Mg_2(dobpdc)	1.073	11.1	2.5	N_2 purge at 393 K	71	S3
en-Mg_2(dobpdc)	0.955	14.6	3.2	Ar purge at 423 K	51	S2
1'	1.227	13.1	3.7	N_2 purge at 358 K	124	This work
2'	1.354	13.4	4.1	N_2 purge at 358 K	120	This work

References

(S1) D. Wu, J. J. Gassensmith, D. Gouvêa, S. Ushakov, J. F. Stoddart, A. Navrotsky, *J. Am. Chem. Soc.* **2013**, *135*, 6790.

(S2) W. R. Lee, S. Y. Hwang, D. W. Ryu, K. S. Lim, S. S. Han, D. Moon, J. Choi, C. S. Hong, *Energy Environ. Sci.* **2014**, *7*, 744.

(S3) T. M. McDonald, W. R. Lee, J. A. Mason, B. M. Wiers, C. S. Hong, J. R. Long, *J. Am. Chem. Soc.* **2012**, *134*, 7056.

(S4) T. M. McDonald, D. M. D'Alessandro, R. Krishna, J. R. Long, *Chem. Sci.* **2011**, *2*, 2022.

(S5) P. Nugent, Y. Belmabkhout, S. D. Burd, A. J. Cairns, R. Luebke, K. Forrest, T. Pham, S. Ma, B. Space, L. Wojtas, M. Eddaoudi, M. J. Zaworotko, *Nature* **2013**, *495*, 80.

(S6) X. Si, C. Jiao, F. Li, J. Zhang, S. Wang, S. Liu, Z. Li, L. Sun, F. Xu, Z. Gabelica, C. Schick, *Energy Environ. Sci.* **2011**, *4*, 4522.

(S7) S. R. Caskey, A. G. Wong-Foy, A. J. Matzger, *J. Am. Chem. Soc.* **2008**, *130*, 10870.

(S8) D.-D. Zhou, C.-T. He, P.-Q. Liao, W. Xue, W.-X. Zhang, H.-L. Zhou, J.-P. Zhang, X.-M. Chen, *Chem. Commun.* **2013**, *49*, 11728.

(S9) J. An, S. J. Geib and N. L. Rosi, *J. Am. Chem. Soc.*, 2009, **132**, 38;

(S10) R. Luebke, J. F. Eubank, A. J. Cairns, Y. Belmabkhout, L. Wojtas, M. Eddaoudi, *Chem. Commun.* **2012**, *48*, 1455.

(S11) B. Li, Z. Zhang, Y. Li, K. Yao, Y. Zhu, Z. Deng, F. Yang, X. Zhou, G. Li, H. Wu, N. Nijem, Y. J. Chabal, Z. Lai, Y. Han, Z. Shi, S. Feng and J. Li, *Angew. Chem., Int. Ed.*, 2012, **51**, 1412.

(S12) R. Vaidhyanathan, S. S. Iremonger, K. W. Dawson and G. K. Shimizu, *Chem. Commun.*, 2009, 5230.

(S13) Q. Min Wang, D. Shen, M. Bülow, M. Ling Lau, S. Deng, F. R. Fitch, N. O. Lemcoff, J. Semanscin, *Microporous and Mesoporous Mater.* **2002**, *55*, 217.

(S14) D. Lassig, J. Lincke, J. Moellmer, C. Reichenbach, A. Moeller, R. Glaser, G. Kalies, K. A. Cychosz, M. Thommes, R. Staudt, H. Krautscheid, *Angew. Chem., Int. Ed.* **2011**, *50*, 10344.

(S15) J. R. Li, J. Yu, W. Lu, L. B. Sun, J. Sculley, P. B. Balbuena and H. C. Zhou, *Nat. Commun.*, 2013, **4**, 1538.

(S16) R. B. Lin, D. Chen, Y. Y. Lin, J. P. Zhang and X. M. Chen, *Inorg. Chem.*, 2012, **51**, 9950.

(S16) R. B. Lin, D. Chen, Y. Y. Lin, J. P. Zhang and X. M. Chen, *Inorg. Chem.*, 2012, **51**, 9950.

(S17) B. Zheng, J. Bai, J. Duan, L. Wojtas and M. J. Zaworotko, *J. Am. Chem. Soc.*, 2011, **133**, 748.

(S18) S. Y. Sung and M. P. Suh, *J. Mater. Chem. A*, 2014, **2**, 13245.

(S19) Y. C. Lin, Q. J. Yan, C. L. Kong and L. Chen, *Sci. Rep.* 2013, **3**, 1859.